Mapping the Binding of Synthetic Disaccharides Representing Epitopes of Chlamydial Lipopolysaccharide to Antibodies with NMR[†]

Hannu Maaheimo,[‡] Paul Kosma,[§] Lore Brade,[∥] Helmut Brade,[∥] and Thomas Peters*,[‡]

Institut für Chemie, Medizinische Universität Lübeck, Ratzeburger Allee 160, D-23538 Lübeck, Germany, Institut für Chemie der Universität für Bodenkultur Wien, A-1190 Wien, Austria, and Forschungszentrum Borstel, Zentrum für Medizin und Biowissenschaften, Parkallee 22, D-23845 Borstel, Germany

Received April 5, 2000; Revised Manuscript Received July 27, 2000

ABSTRACT: A NMR study of the binding of the synthetic disaccharides α-Kdo-(2→4)-α-Kdo-(2→O)-allyl **1** (Kdo, 3-deoxy-D-*manno*-oct-2-ulopyranosonic acid) and α-Kdo-(2→8)-α-Kdo-(2→O)-allyl **2**, representing partial structures of the lipopolysaccharide epitope of the intracellular bacteria *Chlamydia*, to corresponding monoclonal antibodies (mAbs) S23-24, S25-39, and S25-2 is presented. The conformations of **1** bound to mAbs S25-39 and of **2** bound to mAbs S23-24 and S25-39 were analyzed by employing transfer-NOESY (trNOESY) and QUIET-trNOESY experiments. A quantitative analysis of QUIET-trNOESY buildup curves clearly showed that S25-39 recognized a conformation of **1** that was similar to the global energy minimum of **1**, and significantly deviated from the conformation of **1** bound to mAb S25-2. For disaccharide **2**, only a qualitative analysis was possible because of severe spectral overlap. Nevertheless, the analysis showed that all mAbs most likely bound to only one conformational family of **2**. Saturation transfer difference (STD) NMR experiments were then employed to analyze the binding epitopes of the disaccharide ligands **1** and **2** when binding to mAbs S23-24, S25-39, and S25-2. It was found that the nonreducing pyranose unit was the major binding epitope, irrespective of the mAb and the disaccharide that were employed. Individual differences were related to the engagement of other portions of the disaccharide ligands.

Cell surface carbohydrate epitopes are markers of bacteria and cancer cells and, therefore, represent important targets for diagnostic and therapeutic antibodies. To date, the description of how antibodies recognize oligosaccharides at a molecular level has been the subject of a limited number of studies only. The crystal structures of a dodecasaccharide of the O-antigen from the cell surface-exposed LPS[1] of *Salmonella enterica* serogroup B (*1*) and its trisaccharide fragment (*2*) as well as a synthetic pentasaccharide fragment of the O-antigen of *Shigella flexneri* (*3*) have been determined in complexes with Fab or Fv fragments. The solution structure of the *Salmonella* trisaccharide−Fab complex was also studied by NMR (*2*), and recently, it was shown by transferred NOE experiments that a glycosidic linkage in a *Salmonella* type pentasaccharide adopts an anti conformation to avoid unfavorable contacts with the protein surface when bound by an antibody single-chain Fv fragment (*4*). Also, the estrone−3-glucuronide glycoconjugate is bound in a high-energy conformation by an antibody Fv fragment (*5*). From these studies, it appears that the energetically most favorable conformation of a carbohydrate antigen in solution is not necessarily the one that is bound by the protein.

We are studying the binding of antibodies to the LPS of *Chlamydia*, obligatory intracellular pathogens, which cause a broad spectrum of diseases in humans and animals (*6*−*8*). Chlamydial LPS is one of the major surface antigens of these Gram-negative bacteria containing unique sequences of Kdo monomers not found in any other organism. Whereas the trisaccharide α-Kdo-(2→8)-α-Kdo-(2→4)-α-Kdo **3** has been detected in different species of the genus *Chlamydia*, the trisaccharide α-Kdo-(2→4)-α-Kdo-(2→4)-α-Kdo and the branched tetrasaccharide α-Kdo-(2→4)-[α-Kdo-(2→8)]-α-Kdo-(2→4)-α-Kdo have been found in the LPS of *Chlamydia psittaci* (*9*). These saccharides represent *Chlamydia*-specific epitopes, and therefore, corresponding antibodies are used for the diagnosis of chlamydial infections (*10*).

Both disaccharide elements, α-Kdo-(2→8)-α-Kdo and α-Kdo-(2→4)-α-Kdo, exist as terminal structural components in chlamydial antigens. To better understand their interaction with mAbs, we subjected two synthetic disaccharides α-Kdo-

[†] This work was financially supported by grants from the Deutsche Forschungsgemeinschaft DFG (SFB470, projects B3 and C1), from the Fonds der Chemischen Industrie (VCI), and from the Bundesministerium für Bildung und Forschung BMBF (BMBF 0311361). Support came also from the Academy of Finland (to H.M., Grant 56809) and from the Finnish Cultural Foundation (to H.M.). P.K. thanks the Austrian government for a grant (FWF, P 13843-CHE).

* To whom correspondence should be addressed. Phone: +49-451-500-4230. Fax: +49-451-500-4241. E-mail: thomas.peters@chemie.mu-luebeck.de.

[‡] Medizinische Universität Lübeck.

[§] Institut für Chemie der Universität für Bodenkultur Wien.

[∥] Zentrum für Medizin und Biowissenschaften.

[1] Abbreviations: BSA, bovine serum albumin; ELISA, enzyme-linked immunosorbent assay; I-BURP, inversion band-selective uniform response pure phase pulse; Kdo, 3-deoxy-D-*manno*-oct-2-ulopyranosonic acid; LPS, lipopolysaccharide; mAb, monoclonal antibody; MMC, Metropolis Monte Carlo; NOESY, nuclear Overhauser effect spectroscopy; QUIET-trNOESY, quenching of undesirable indirect external trouble in trNOESY; trNOE, transfer nuclear Overhauser effect; trNOESY, transfer nuclear Overhauser effect spectroscopy; STD, saturation transfer difference.

10.1021/bi000780o CCC: $19.00
Published on Web 09/28/2000

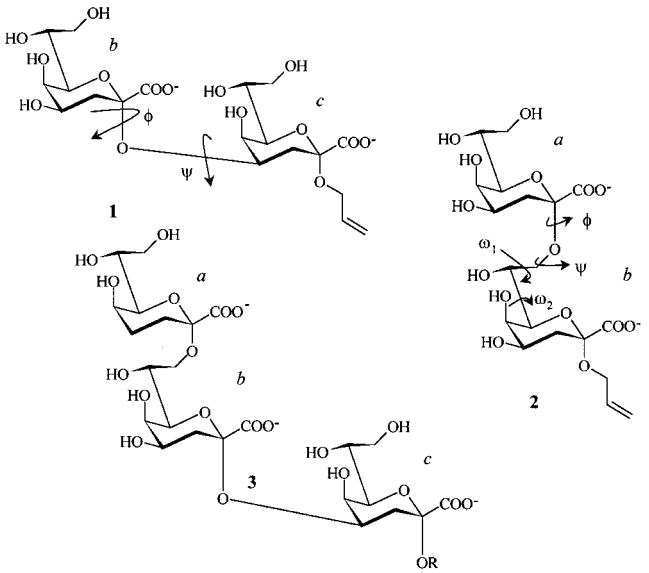

FIGURE 1: Structures of the saccharides α-Kdo-(2→4)-α-Kdo-(2→O)-allyl **1**, α-Kdo-(2→8)-α-Kdo-(2→O)-allyl **2**, and α-Kdo-(2→8)-α-Kdo-(2→4)-α-Kdo **3**. Dihedral angles at glycosidic linkages are explained (ϕ, ψ, ω_1, and ω_2). The pyranose rings are labeled a, b, and c.

(2→4)-α-Kdo-(2→O)-allyl **1** and α-Kdo-(2→8)-α-Kdo-(2→O)-allyl **2** (Figure 1) to detailed conformational analyses in the free state and when they were bound to *Chlamydia*-specific mAbs S25-2 and S23-24 (*11*, *12*). One problem for the NMR analysis was a severe overlap of proton resonances which was especially unfavorable for disaccharide **2**. In solution, both disaccharides exist as a mixture of several conformational families. S25-2 recognized a conformation of **1** that was not highly populated in solution (*11*). For **1** bound to S23-24, it was impossible for individual conformations to fulfill all distance constraints obtained from trNOE experiments. Therefore, it was concluded that at least two different conformations of **1** were bound to S23-24 (*11*). To summarize, mAbs S23-24 and S25-2 recognized notably different conformations of **1**. When **2** binds to mAb S25-2, a conformation was selected that was also highly populated in solution (*12*).

Here, we continue our studies on the recognition of oligosaccharide antigens by *Chlamydia*-specific mAbs. Conformational analyses of disaccharide **2** bound to mAb S23-24 and of both disaccharides **1** and **2** bound to mAb S25-39 are presented. A subsequent determination of the binding epitopes of both disaccharides **1** and **2** bound to mAbs S25-39, S25-2, and S23-24 is based on saturation transfer difference (STD) NMR spectroscopy, a technique that has been introduced recently (*13*).

MATERIALS AND METHODS

Monoclonal Antibodies and Serology. mAb S25-2 (IgG1 isotype) has been described previously (*15*). From the same fusion, an additional antibody (IgG1 isotype) was selected, termed S25-39. Antibody S23-24 (IgG1 isotype) was obtained after immunization of mice with a neoglycoconjugate containing as a carbohydrate ligand the deacylated lipopolysaccharide from recombinant *Salmonella enterica* serovar Minnesota R595 expressing the 3-deoxy-D-*manno*-oct-2-ulosonic acid transferase of *Chlamydia trachomatis*. Erroneously, this antibody has been reported as being obtained after immunization with the synthetic tetrasaccharide α-Kdo-(2→8)-α-Kdo-(2→4)-α-Kdo-(2→6)-β-GlcNAc (*15*). Culture supernatants of the respective hybridomas were purified and concentrated by affinity chromatography using as immobilized ligands α-Kdo-(2→8)-α-Kdo-(2→4)-α-Kdo-(2→6)-βGlcNAc-(1→6)-αGlcNAc 1,4′-P_2 for mAbs S25-2 and S25-39 and α-Kdo-(2→4)-α-Kdo-(2→6)-βGlcNAc-(1→6)-αGlcNAc 1,4′-P_2 (*14*) for mAb S23-24 as described previously (*17*).

Attachment of mAbs to immobilized ligands was assessed by ELISA using neoglycoconjugates. Neoglycoconjugates were obtained after spacer extension of **1** and **2** by addition of cysteamine followed by activation with thiophosgen into the isothiocyanate derivative and conjugation to BSA. Details of the assay format have been described previously (*17*). Briefly, varying amounts of neoglycoconjugate antigens were coated onto 96-well microtiter plates and tested against serial dilutions of antibody. The reaction was developed by incubation with enzyme-conjugated anti-mouse IgG and substrate, and assessed photometrically at 405 nm. Experiments were set up in quadruplicates, and mean values were calculated. Confidence values did not exceed 10%.

The mAbs in this study were obtained after immunization with oligosaccharides conjugated to BSA. We selected only those antibodies that recognized the carbohydrate ligands in different chemical and physicochemical environments. For instance, the antibodies were able to bind to chlamydial LPS as present in the bacterial outer membrane (assessed via immunofluorescence), to recombinant LPS (assessed via hemagglutination assays, ELISA, and Western and dot blot), to neoglycoconjugates, and to polyacrylamide copolymers (*15*). In addition, the allyl glycosides can be used in competitive inhibition assays using either LPS or conjugates as the solid-phase antigen.

Sample Preparation. The disaccharides α-Kdo-(2→4)-α-Kdo-(2→O)-allyl **1** and α-Kdo-(2→8)-α-Kdo-(2→O)-allyl **2** were available from synthesis as previously described (*18*). The antibodies were transferred into 10 mM sodium acetate-d_3 buffer (99.9% D, pH 4.0) using Centricon filters (excluding molecular mass of 100 kDa, Amicon). The protein concentration was determined with the Bradford test (Bioquant, Merck) (*19*) using bovine IgG as a standard. In the final experiments, the molar ratio of mAb binding sites to carbohydrate ligand was 1:12, which was found in control experiments to be close to the optimum ratio. The individual samples were as follows: 20 nmol (40 nmol of binding sites) of mAb S23-24 and 480 nmol of saccharide **2**, 17 nmol (34 nmol of binding sites) of mAb S25-39 and 408 nmol of saccharide **2**, and 34 nmol (68 nmol of binding sites) of mAb S25-39 and 816 nmol of saccharide **1**. In each case, the sample volume was 0.5 mL.

NMR Experiments. The NMR experiments were performed on Bruker Avance DRX500 and DRX600 spectrometers. All spectra were acquired at 310 K without sample spinning, and the HDO signal was used as an internal reference (4.65 ppm at 310 K). XWINNMR software (Bruker) running on Silicon Graphics workstations was used for data acquisition and processing.

Two-dimensional trNOESY experiments with disaccharide **2** were performed at 600.13 MHz, and those with disaccharide **1** were performed at 500.13 MHz. A total of 512 (t_1) ×

4K (t_2) data points were recorded for each experiment. Prior to Fourier transformation, the data matrix was multiplied with a squared cosine function. The spectral width was 6.61 ppm. The HDO signal was suppressed by low-power presaturation during the relaxation and mixing time. The total relaxation delay was 1.5 s. Mixing times of 200 and 250 ms were used. To suppress the protein signals, a spin-lock field of 5 kHz with a duration of 10 ms was applied after the first 90° pulse (*20*). Thirty-two dummy scans and 64 scans per increment were performed.

Two-dimensional QUIET-trNOESY experiments (*21*) were performed at 500.13 MHz using a modified NOESY pulse sequence (*11*). Protein signals were suppressed by a 5 kHz spin-lock field with a duration of 10 ms after the first 90° pulse (*20*). In the middle of the mixing time, a double-selective I-BURP inversion pulse was applied. The programs xShape and Mule (Bruker) were used to generate the double-selective pulse shape. A homospoil gradient (1 ms, 5 G/cm) was used at the end of the mixing time to improve the spectral quality. A total of 512 (t_1) × 2K (t_2) data points were recorded. Prior to Fourier transformation, the data matrix was zero-filled to a 1K × 4K matrix, and multiplied with a squared cosine function. The spectral width was 10 ppm. The HDO signal was suppressed by low-power presaturation during the relaxation and mixing time. The total relaxation delay was 1.4 s, and the mixing times were 80, 150, 250, 350, 450, and 600 ms.

The baselines of the QUIET-trNOESY spectra were corrected in F_2 and F_1 (third-order polynomial) prior to integration of cross-peak volumes. Integration and calculation of initial slopes were performed with the program AURELIA (*22*). Experimental trNOE curves were fitted to a double-exponential function, $f(t) = p_0 e^{-p_2 t}(1 - e^{-p_1 t})$, where p_0, p_1, and p_2 are adjustable parameters. The initial slope was determined from the first derivative at time zero, $f'(0) = p_0 p_1$, and the interproton distances were obtained from the initial slopes employing the isolated spin-pair approximation using a distance of 2.45 Å (*14*) between protons H4^c and H6^c as a reference.

One-dimensional STD NMR experiments (*13*, *23*−*25*) were recorded with a 5 kHz spin-lock field with a duration of 10 ms. Saturation transfer was achieved by using 40 selective Gaussian 270° pulses with a duration of 50 ms and a spacing of 10 ms. For one set of spectra, the protein envelope was irradiated at 0.97 ppm (on-resonance) and −2 ppm (off-resonance). Another set of spectra was generated by setting the on-resonance frequency to 7.11 ppm. Subsequent subtraction was achieved via phase cycling. Saturation times were 0.25, 0.5, 0.75, 1.0, 1.5, and 2.0 s. The relaxation delay was set at 0.5 s. The acquisition time was 2 s. Typically, 128 or 512 scans were recorded with 64 dummy scans each. The samples used for all STD experiments were partly identical with the ones used for the trNOE experiments. New samples were prepared with a larger excess of ligand. The sample compositions were as follows: mAb S23-24 (5.8 nmol) in the presence of a 64-fold excess of disaccharide **2** (740 nmol); mAb S25-2 in the presence of disaccharide **2**, as used for the trNOE experiments (*12*); mAb S25-39 in the presence of disaccharide **2**, as used for the trNOE experiments (see above); mAb S23-24 (10.6 nmol) in the presence of a 50-fold excess of disaccharide **1** (1060 nmol); mAb S25-2 in the presence of disaccharide **1**, as used for the trNOE experiments (*11*); and mAb S25-39 (6.2 nmol) in the presence of a 68-fold excess of disaccharide **1** (848 nmol).

Table 1: Upper and Lower Distance Constraints for α-Kdo-(2→4)-α-Kdo-(2→O)-allyl **1** Bound to mAb S25-39[a]

	lower distance (Å)	upper distance (Å)
H6^b−H4^c	1.98	2.96
H8proR^b−H4^c	2.40	3.60
H6^b−H3ax^c	2.74	4.12
H6^b−H3eq^c	2.76	4.14
H8proR^b−H3eq^c	3.00*	5.50*
H8proS^b−H3eq^c	3.00*	5.50*

[a] All values except the ones marked with an asterisk (*) were derived from trNOE buildup curves by adding an estimated experimental error of ±20% to the distance that was obtained. For the proton pairs marked with an asterisk (*), reliable buildup curves could not be obtained due to the weakness of the signals, and the values are generous estimates.

TOCSY and STD TOCSY spectra were recorded with 256 increments and 32 transients using a MLEV-17 spin-lock field of 50 ms at 7.5 kHz. The relaxation delay was set at 0.6 s. Saturation transfer was achieved by using 40 selective Gaussian 270° pulses with a duration of 50 ms and a spacing of 10 ms. The protein envelope was irradiated at 7.11 or 0.97 ppm (on-resonance) and 40 ppm (off-resonance). Protein presaturation was applied for 1 s. Subsequent subtraction of on- and off-resonance spectra was achieved via phase cycling.

For STD NMR experiments, the following control experiments have been performed. (1) Samples containing only the ligand molecules were subjected to one-dimensional STD NMR experiments using saturation conditions identical to those applied in the one-dimensional STD and STD TOCSY NMR experiments with the ligands in the presence of mAbs. The resulting difference spectra did not contain any signals, showing that saturation transfer via the protein was the sole reason for the effects observed using samples with the ligand molecules in the presence of mAbs. (2) Difference spectroscopy was performed via phase cycling. In conjunction with the excellent stability of our magnet, no subtraction artifacts were expected. This was experimentally demonstrated by subtracting on-resonance spectra from on-resonance spectra, or off-resonance spectra from off-resonance spectra. The resulting one- or two-dimensional spectra contained no signals. (3) The frequencies for protein saturation were determined from STD experiments with samples containing mAbs only. Frequencies were chosen such that protein signals in the difference spectra were optimal, at the same time avoiding interference with ligand signals (see above).

Computational Methods. Metropolis Monte Carlo (MMC) simulations were performed with the program GEGOP on a Silicon Graphics O2 R10000 workstation (*26*, *27*). The glycosidic bond angles were fixed at 117°, and the pyranose rings were treated as rigid units in the $^5C_2$ conformation. The dihedral angles ϕ and ψ at the glycosidic linkages and ω_1 and ω_2 at the side chains were defined as follows: ϕ, C1′−C2′−O*x*−C*x*; ψ, C2′−O2′−C*x*−H*x*; ω1, C8−C7−C6−C5; and ω2, O8−C8−C7−C6, with *x* being the aglyconic linkage site (Figure 1). The temperature parameter was set at 2000 K to efficiently sample accessible conformational space. A total of 2×10^6 macro steps were calculated for each simulation.

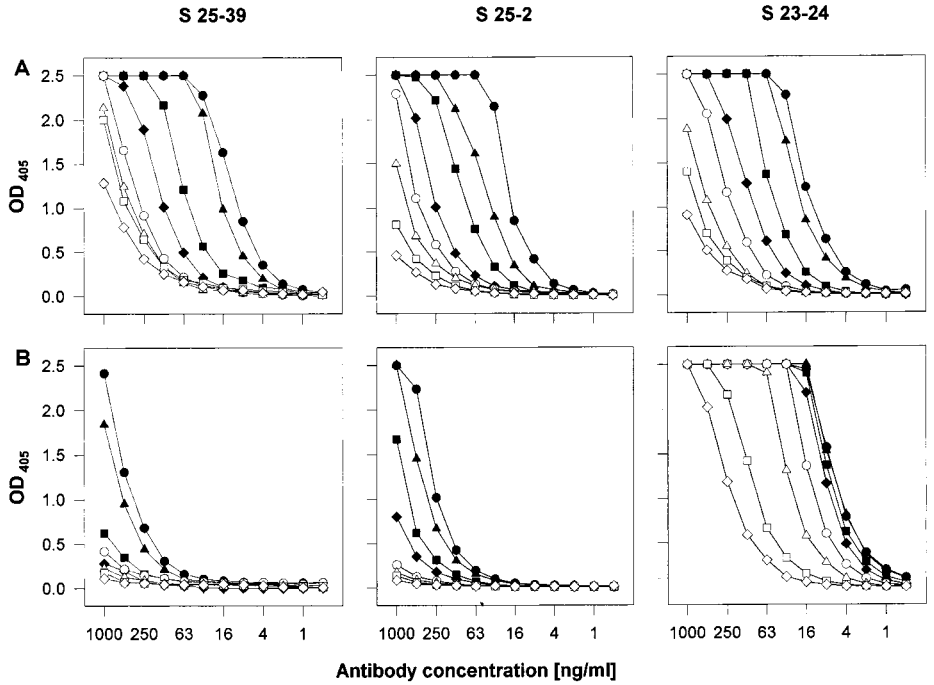

FIGURE 2: Binding curves (semilogarithmic) of mAbs S23-24 (IgG_1), S25-2 (IgG_1), and S25-39 (IgG_1) with neoglycoconjugates containing the disaccharides α-Kdo-(2→8)-α-Kdo (A) and α-Kdo-(2→4)-α-Kdo (B), representing partial structures of chlamydial LPS. ELISA plates were coated with graded concentrations of neoglycoconjugates corresponding to 400 (●), 200 (▲), 100 (■), 50 (◆), 25 (○), 12.5 (△), 6.3 (□), and 3.2 (◇) pmol of ligand/mL using 50 μL per well and reacted with monoclonal antibodies at the indicated concentrations on the abscissa. Values are the mean of quadruplicates with confidence values not exceeding 10%. The curves show that binding affinities of the mAbs to the 2→8-linked disaccharide were very similar (A). For the 2→4-linked disaccharide, mAb S23-24 had the highest binding affinity (B, rightmost curves). A comparison of the antibody concentrations at an OD of 1.5 shows that the affinity of binding of S23-24 for the 2→4-linked disaccharide was 20−50-fold higher than the affinity of binding mAbs S25-39 and S25-2 to this disaccharide (B). A comparison of panels A and B clearly demonstrates that mAbs S25-39 and S25-2 discriminate well between the 2→8- and the 2→4-linked disaccharide, whereas this discrimination is not very pronounced for mAb S23-24.

The bound conformation of disaccharide **1** was deduced from the interproton distances obtained from the experimental QUIET-trNOESY buildup curves. First, an estimated experimental error of ±20% was added, and the distances that were obtained were used as upper and lower bounds. All conformations fulfilling these constraints were then extracted from the 2000 K MMC calculation. The constraints are summarized in Table 1.

RESULTS AND DISCUSSION

The NMR experiments described herein aim at the analysis of the bioactive conformations of disaccharides α-Kdo-(2→4)-α-Kdo-(2→O)-allyl **1** and α-Kdo-(2→8)-α-Kdo-(2→O)-allyl **2** when they are bound to mAb S25-39. A qualitative analysis of the bioactive conformation of **2** when complexed with mAb S23-24 is also presented. For the analysis of bioactive conformations, trNOESY experiments were utilized. To define the binding epitopes of the carbohydrate ligands, we performed STD NMR experiments (*13*, *23*−*25*) for disaccharides **1** and **2** complexed with mAb S25-39, S25-2, or S23-24. STD NMR experiments have been introduced lately as a tool for screening compound mixtures for binding activity (*13*, *23*−*25*) and for determining binding epitopes (*13*). The NMR experiments were complemented by the determination of relative binding affinities of the mAbs toward the 2→8-linked and the 2→4-linked disaccharide units utilizing ELISA.

Determination of Relative Binding Affinities of mAbs S25-39, S25-2, and S23-24. The binding affinities of mAbs S25-39, S25-2, and S23-24 toward the 2→8- and 2→4-linked Kdo disaccharides, conjugated to bovine serum albumin, and immobilized on microtiter plates were determined using an ELISA system. The mAbs recognized the carbohydrate ligands in different chemical and physicochemical environments (*15*). The resulting binding curves are shown in Figure 2. Binding to the immobilized 2→8-linked Kdo disaccharide was comparable for all three mAbs, as this is clearly seen from Figure 2A. Significant differences were observed for the binding to the immobilized 2→4-linked Kdo disaccharide (Figure 2B). Whereas mAb S23-24 bound to the 2→4-linked disaccharide with high affinity (Figure 2B, right panel), mAbs S25-39 and S25-2 bound to this ligand only at high antibody and antigen concentrations (Figure 2B, left and center panels). From a qualitative comparison of the binding curves in Figure 2B, it was obvious that the affinities of mAbs S25-39 and S25-2 were approximately 20−50-fold lower than the binding affinity of mAb S23-24. A comparison of the binding curves in row A of Figure 2 with those of row B also showed that mAbs S25-39 and S25-2 discriminate well the 2→8-linked from the 2→4-linked disaccharide, whereas this discrimination was not very pronounced for mAb S23-24.

*Conformation of α-Kdo-(2→8)-α-Kdo-(2→O)-allyl **2** Bound to mAbs S23-24 and S25-39.* An analysis of the conformation of **2** bound to mAb S25-2 has been published previously (*12*). A number of interglycosidic trNOEs were key to deducing a family of possible bound conformations. These trNOEs, $\{H4^{a}-H2^{allyl}\}$, $\{H6^{b}-H2^{allyl}\}$, $\{H4^{a}-H3z^{allyl}\}$, $\{H6^{a}-$

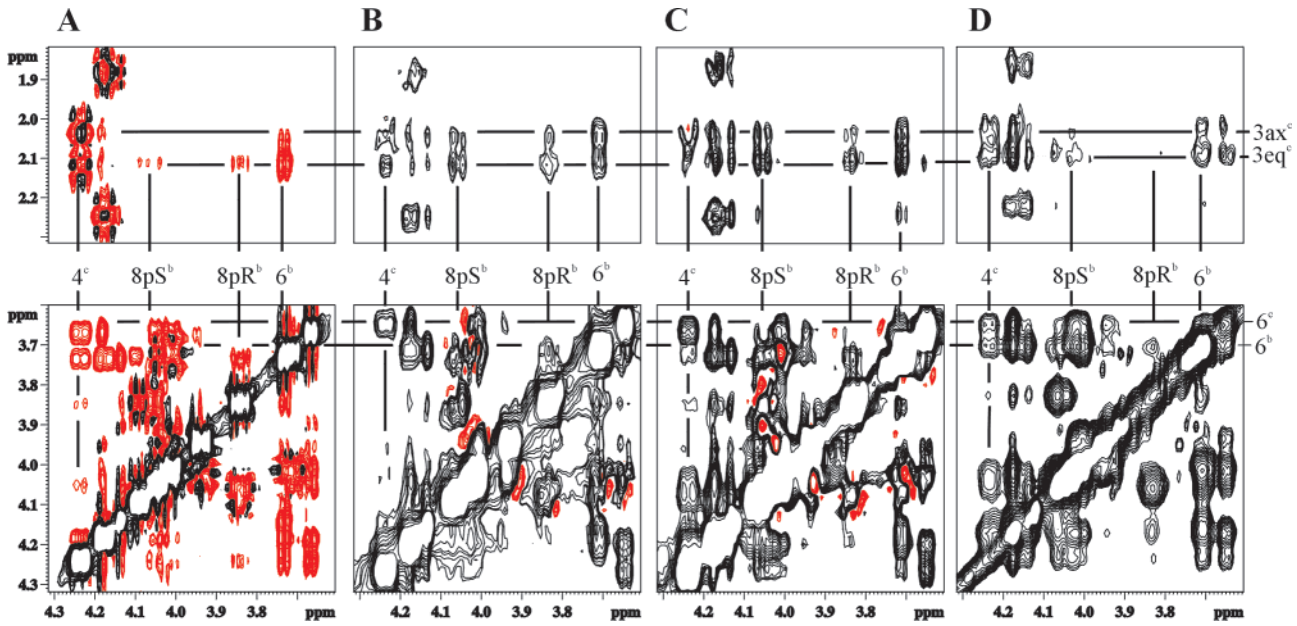

FIGURE 3: Expansions of the 500 MHz NOESY and trNOESY spectra of α-Kdo-(2→4)-α-Kdo-(2→O)-allyl **1**. By definition, black contours are negative signals and red contours are positive signals. (A) NOESY spectrum of **1** in aqueous solution. (B−D) trNOESY spectra of **1** complexed with mAb S25-2 (B), S23-24 (C), and S25-39 (D). Each spectrum exhibits a clearly different cross-peak pattern reflecting the different conformations of **1** in solution and in each complex. Spectra A−C are from ref *11*. For the conformational analysis of **1** bound to mAbs, the trNOE cross-peak between $H4^c$ and $H6^b$ is very important. In spectrum D (**1** bound to mAb S25-39), this cross-peak has the largest relative intensity, indicating that a conformation of **1** close to the global minimum is bound (cf. Table 2).

$H8^b$}, {$H6^a$−$H1^{allyl}$}, and {$H6^b$−$H3z^{allyl}$}, were also observed for **2** in the presence of mAb S23-24 or S25-39 (corresponding trNOESY spectra are available as Supporting Information). Therefore, we concluded that the bioactive conformation of **2** bound to mAb S23-24 or S25-39 is within the range of bound conformations determined previously for **2** complexed with mAb S25-2 (*12*).

Some of the trNOE cross-peaks, e.g., {$H4^b$−$H8^b$} and {$H4^a$,$H5^b$−$H8^b$}, that were observed for disaccharide **2** bound to mAb S25-2 had been shown to be due to spin diffusion via protein protons (*12*). These cross-peaks were also present in the trNOESY spectrum of disaccharide **2** in the presence of mAb S25-39. However, their intensity was reduced when **2** bound to mAb S23-24. The cross-peak {$H4^b$−$H8^b$} was absent, and the intensity of the cross-peak {$H4^a$,$H5^b$−$H8^b$} was notably reduced. This reduction in the level of spin diffusion may reflect differences in the geometry of the binding pocket of the protein, or in the geometry of the bound ligand.

*Conformation of α-Kdo-(2→4)-α-Kdo-(2→O)-allyl **1** Bound to mAb S25-39.* The conformations of **1** bound to mAbs S25-2 and S23-24 have been investigated (*11*). The trNOESY spectrum of **1** in the presence of S25-39 exhibited strong negative trNOEs, and the cross-peak pattern was clearly different from those of **1** bound to mAb S25-2 or S23-24 (Figure 3). A strong trNOE between protons $H6^b$ and $H4^c$ (for notations of the pyranose rings, cf. Figure 1) indicated that a conformation closely related to the global minimum energy conformation A (Table 2) was bound. This trNOE was absent from the trNOESY of disaccharide **1** in the presence of S25-2, and had a much reduced intensity for **1** binding to mAb S23-24 (Figure 3). In the trNOESY spectrum of disaccharide **1** bound to mAb S25-39, trNOEs from proton $H8proR^b$ or $H8proS^b$ to the protons attached to C3 of pyranose ring c were very weak (Figure 3), and almost absent

Table 2: Conformations of α-Kdo-(2→4)-α-Kdo-(2→O)-allyl **1** Obtained from MMC Simulations[a]

conformation	ϕ/ψ (deg)[b]	relative energy (kcal/mol)	mAb which recognizes **1**
A	−78/−26	0.0	S23-24
A′	−69/−44	4.9	S25-39
B	−52/5	0.2	S23-24
C	−44/33	4.8	S25-2, S23-24
D	62/8	3.2	−

[a] The mAbs that recognize the individual conformations are also summarized. [b] Errors were estimated as ±15°.

in a QUIET-trNOESY spectrum. This was very different from the trNOEs observed for **1** bound to mAb S25-2 or S23-24. We concluded that conformations similar to minimum B or C (Table 2) did not represent the conformation of **1** bound to mAb S25-39. Otherwise, these latter trNOEs would have been of significant size (*11*). This qualitative analysis already strongly suggested that a conformation similar to the global minimum A was bound to mAb S25-39. To further substantiate this conclusion, we performed a quantitative analysis as this had been described previously (*11*).

A correct interpretation of trNOEs requires a detailed analysis of spin-diffusion pathways. It has been argued that a major source of error is the presence of spin diffusion via protein protons (*21*, *28*−*30*). Spin-diffusion effects in ligand−protein complexes are effectively suppressed by carrying out band-selective QUIET-trNOESY experiments (*21*). Therefore, we acquired QUIET-trNOE buildup curves to allow a quantitative interpretation of the data. A double-selective I-BURP pulse was applied during the mixing time to invert the resonances in the spectral regions of 4.29−3.57 and 2.42−1.70 ppm. Since the resonances of the aromatic and most of the aliphatic amino acid side chain protons were excluded from this inversion, any spin diffusion

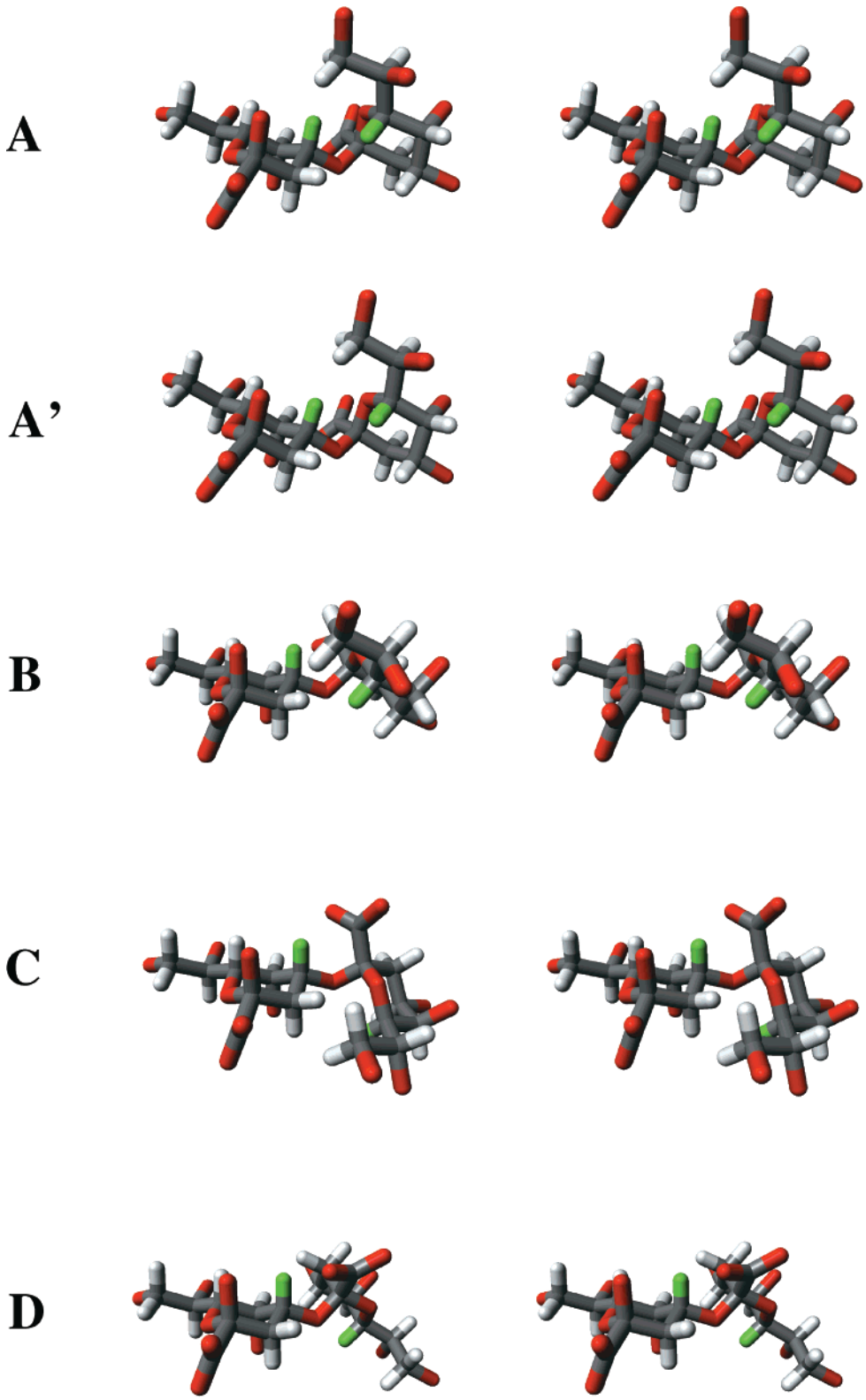

FIGURE 4: Stereoplots of different conformations of α-Kdo-(2→4)-α-Kdo-(2→O)-allyl **1**. The allyl group is not shown. Protons H4^{c} and H6^{b} are depicted in green. Minima A−D correspond to the ones in Table 2. In this study, it was shown that conformation A′ which is similar to the global energy mimimum A was bound by mAb S25-39. mAb S25-2 recognized conformations similar to C, and mAb S23-24 recognized at least two families of conformations (Table 2).

mediated by these protons was neutralized. A series of six QUIET-trNOESY experiments with mixing times ranging from 80 to 600 ms furnished trNOE buildup curves of excellent quality (buildup curves are available as Supporting Information). Only the rather weak trNOEs {H8*pro*R^{b}−H3eq^{c}} and {H8*pro*S^{b}−H3eq^{c}} did not allow a precise integration. From the initial slopes of the trNOE buildup curves, interproton distances were calculated using the intraglycosidic trNOE between H4^{c} and H6^{c} as a reference (see also Materials and Methods). An estimated experimental error was added to the calculated proton−proton distances, furnishing upper and lower distance constraints (Table 1).

For the H8*pro*R^b−H3eq^c and H8*pro*S^b−H3eq^c proton pairs, only rather weak trNOEs were observed, and consequently, initial slopes were not determined. Therefore, rather generous distance constraints of 3.00−5.50 Å were used (Table 1). In general, we estimated the experimental error from the rms deviation of measured cross-peak integrals from the fitted buildup curves. This analysis gave less than ±10% error when transformed to interproton distances, assuming a r^{-6} dependence of trNOEs. Alternatively, the experimental error was analyzed by comparing trNOEs between pairs of protons with fixed distances. In the present case, two intraglycosidic trNOEs, {H4^c−H6^c} and {H3ax^c−H3eq^c}, were suitable for this analysis. Using the distance between H4^c and H6^c as a reference, a value of 2.2 Å was obtained for the distance between H3ax^c and H3eq^c. This was a very reasonable value for the distance between two geminal protons. We decided to apply error limits of ±20% so that so-called virtual bound conformations were not generated.

The distance constraints from Table 1 were then applied to extract bound conformations from a 2000 K MMC simulation as described previously (*11*). This analysis led to a bound conformation A′ that is structurally related to the global minimum A but displays "distortions" of the ϕ and especially the ψ angle. Qualitatively, this distortion is reflected by the relative size of trNOEs {H6^b−H3ax^c} and {H6^b−H3eq^c}. In conformation A, the corresponding distances should significantly differ from each other, yielding values of 2.3 (H6^b−H3eq^c) and 3.7 Å (H6^b−H3ax^c). However, the QUIET-trNOESY buildup curves for trNOEs {H6^b−H3ax^c} and {H6^b−H3eq^c} were almost identical (see the Supporting Information). Conformations A and A′ are shown in Figure 4.

In Table 2, relative energies of the different conformations of **1** are summarized. It is seen that A′ has a rather high relative energy of 4.9 kcal/mol. Our technique of deducing bound conformations always furnishes an ensemble of bound conformations which roughly reflects the accuracy with which a bound conformation may be resolved. In the present case, our analysis showed that ϕ covers a range of ca. ±15°, whereas ψ covers ca. ±10°. This includes bound conformations that are more similar to the global minimum A and, consequently, have a lower energy.

For mapping the binding epitope of disaccharide **1** bound to mAb S25-39, it is interesting to note that intraglycosidic trNOEs were observed between H6^c and both protons attached to C3^c. The effects were not observed for **1** bound to mAb S25-2, or S23-24. These trNOEs were probably due to spin diffusion, suggesting that Kdo unit c is in intimate contact with the protein binding site.

We conclude that the conformation of disaccharide **1** when bound to mAb S25-39 is best described by A′ with a tolerance of ±15° for both dihedral angles at the glycosidic linkage (Table 2). Obviously, this includes conformations that are very similar to A. To summarize, mAbs S25-39, S25-2, and S23-24 each recognize disaccharide **1** in an individual and distinct binding mode. Conformations A and A′ are shown in Figure 4 to depict the range of possible bound conformations of **1** bound to S25-39. To enable a comparison with the other conformations discussed above, conformations B−D are also depicted.

STD NMR Experiments for Epitope Mapping. In general, it is very important to know the size and the shape of the binding epitope of a ligand bound to a receptor protein. As described above, trNOE experiments deliver the shape of the bound ligand, but they provide only limited information about the size of the binding epitope. It has been demonstrated recently that STD NMR is well suited for the analysis of binding epitopes (*13*). STD NMR experiments rely on simple principles. A sample is required that contains a ligand in excess over a receptor protein that binds to the ligand. In a first experiment, a ^{1}H NMR spectrum is recorded with presaturation of the protein signal envelope at a frequency where no ligand protons resonate (on-resonance spectrum). A second spectrum is recorded with the presaturation frequency set at a value that is significantly apart from all resonance frequencies of either the protein or the ligand (off-resonance spectrum). Subtraction of the two spectra leads to a difference spectrum that contains only signals resulting from saturation transfer. Clearly, the whole protein spectrum is visible because magnetization is very effectively distributed via spin diffusion within the protein. It is more important, however, that the magnetization is also transferred to ligand molecules binding to the protein. Clearly, saturation transfer will be more efficient for those parts of the ligand that are

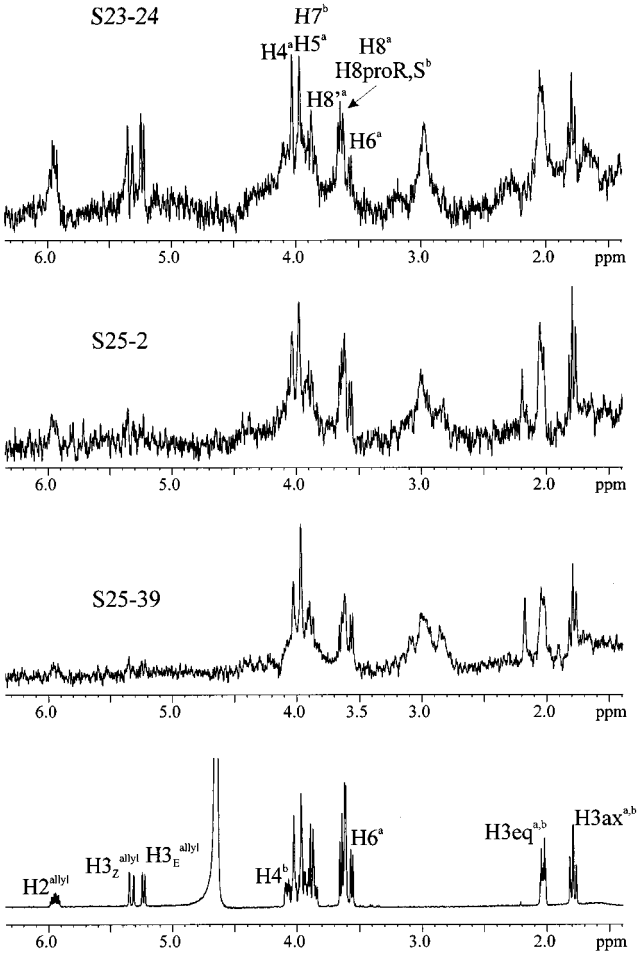

FIGURE 5: One-dimensional STD NMR spectra of disaccharide **2** in the presence of mAbs S23-24, S25-2, and S25-39 (from top to bottom). At the bottom, a ^{1}H NMR spectrum of **2** is shown for reference purposes. Protons H3eq and H3ax of pyranose rings a and b have identical chemical shifts and cannot be discriminated. It is seen that the STD spectra are similar except for the saturation transfer to the protons of the allyl group, only observed for mAb S23-24 (top spectrum). Assignments are given for the top and bottom spectra.

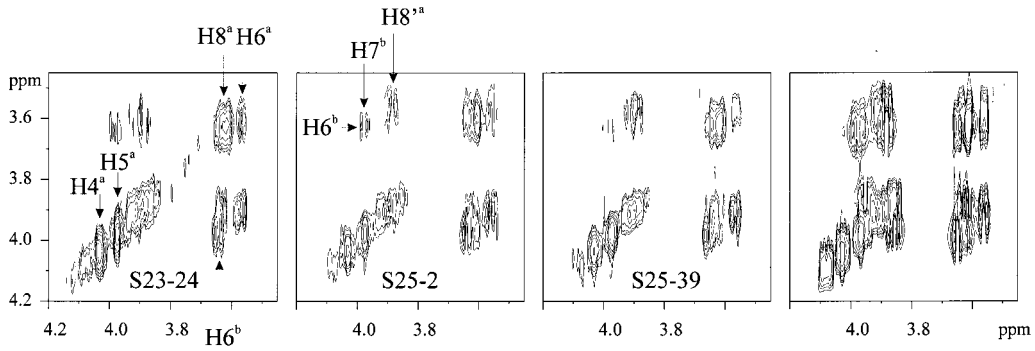

FIGURE 6: Portions of STD TOCSY spectra of disaccharide **2** in the presence of mAbs S23-24, S25-2, and S25-39 (from left to right). The rightmost spectrum is a TOCSY spectrum of **2** for reference purposes. Prominent cross-peaks indicating saturation transfer to the corresponding protons are observed between protons $H7^b$ and $H6^b$, as well as between $H8'^a$ and $H8^a$, irrespective of the mAb employed. $H5^a$ has very small vicinal coupling constants, and therefore, no TOCSY cross-peaks are observed.

in close contact with the protein binding pocket. Since it is known that spin-diffusion effects in low-molecular mass molecules binding to large proteins are mainly due to protein protons (*21*, *28*−*30*), it is reasonable to assume that saturation transferred to a ligand will experience only limited distribution within the ligand molecule once this has left the binding pocket. Therefore, the relative intensities of STD signals contain critical information about the size of the binding epitope of the ligand. Oligosaccharides are especially suitable for this kind of epitope mapping because glycosidic linkages provide bottlenecks for any spin-diffusion process. Therefore, differentiating between pyranose units that are in intimate contact with the protein surface and those that are not is straightforward.

The principle of STD NMR is easily extended to any multidimensional NMR experiment. One very powerful combination is the STD TOCSY experiment (*13*, *23*−*25*) in which presaturation of the protein is performed during the relaxation delay. Subtraction of on- and off-resonance TOCSY spectra may be achieved either by appropriate phase cycling or by subtracting two separate TOCSY data sets. In comparison to one-dimensional STD NMR spectra, STD TOCSY spectra have the advantage that even in regions of severe signal overlap a discrimination of individual resonances is feasible. The presence of a cross-peak in a STD TOCSY spectrum indicates that the corresponding protons are in contact with the protein surface. Usually, all one-dimensional STD spectra are acquired with a spin-lock filter (*20*) after the detection pulse. This removes the protein background and furnishes clean baselines. For STD TOCSY experiments, this is not necessary because the spin-lock field used for isotropic mixing also acts as a spin-lock filter for protein−proton resonances. To ensure that the STD signals that were detected were not due to subtraction artifacts or accidental saturation of ligand molecules, we performed control experiments as described in Materials and Methods.

STD NMR Experiments with α*-Kdo-(2*→*8)-*α*-Kdo-(2*→*O)-allyl* ***2*** *Bound to mAbs S25-2, S25-39, and S23-24.* Spectral overlap was especially severe for the 2→8-linked disaccharide **2**. The protons at C3 of pyranose rings a and b were especially indistinguishable. From one-dimensional STD NMR experiments, it was seen that in the ring proton region the signal patterns were rather similar for all complexes (Figure 5). Prominent signals in the STD spectra were $H6^a$, $H4^a$, and $H5^a$. Protons $H7^b$ and $H5^a$ had identical chemical shifts, and could not be distinguished in a one-dimensional spectrum. In STD TOCSY experiments (Figure 6), cross-peaks between protons $H7^b$ and $H6^b$ were observed for all mAbs, indicating that these two protons were in contact with

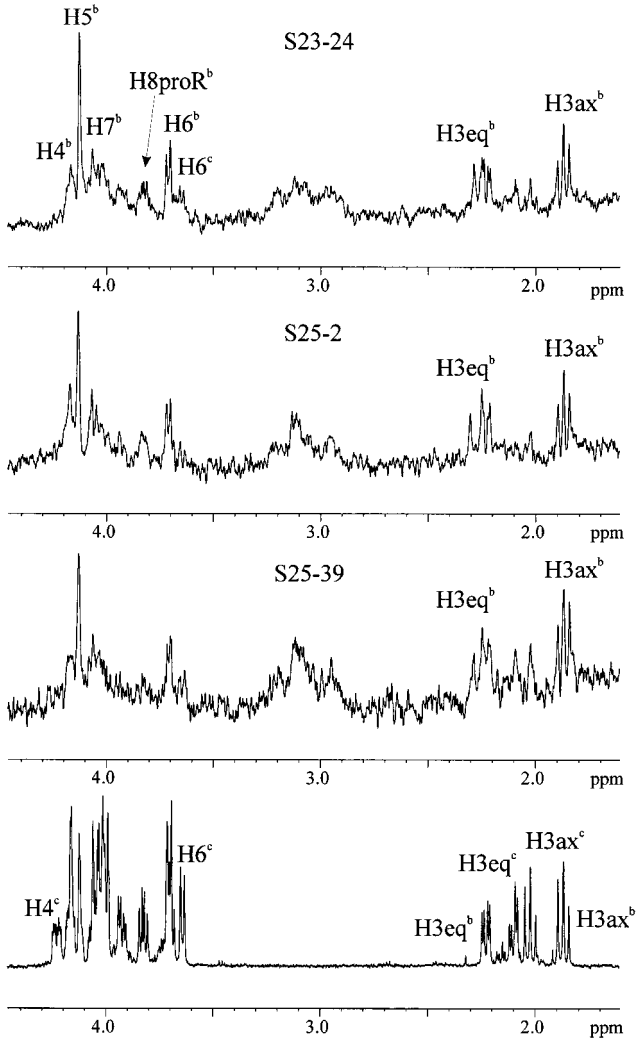

FIGURE 7: One-dimensional STD NMR spectra of disaccharide **1** in the presence of mAbs S23-24, S25-2, and S25-39 (from top to bottom). At the bottom, a ^1H NMR spectrum of **1** is shown for reference purposes. Protons H3eq and H3ax of rings c and b are well separated. It is obvious that in all cases saturation transfer to the protons of the nonreducing pyranose ring b is much more efficient than to those of ring c. The most prominent signals resulting from saturation transfer are $H3ax^b$, $H3eq^b$, $H4^b$, $H5^b$, and $H6^b$, irrespective of the mAb used.

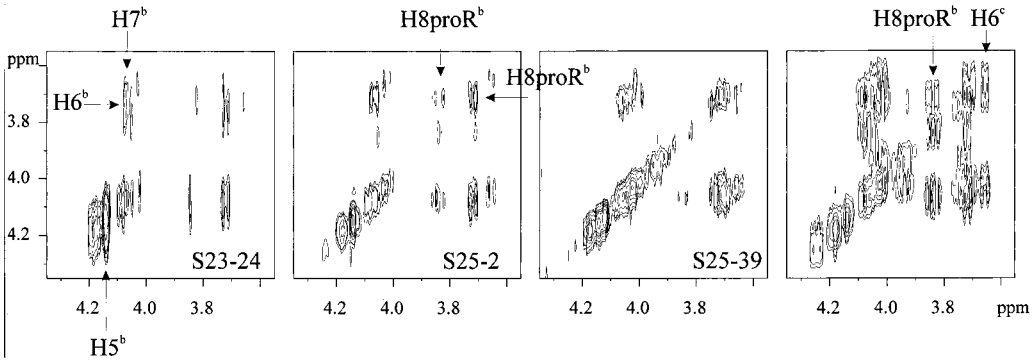

FIGURE 8: Portions of STD TOCSY spectra of disaccharide **1** in the presence of mAbs S23-24, S25-2, and S25-39 (from left to right). The rightmost spectrum is a TOCSY spectrum of **1** for reference purposes. Irrespective of the mAb employed, a cross-peak between protons $H6^b$ and $H7^b$ is observed. The cross-peak between H8*pro*R^b and H8*pro*S^b is less intense. It appears that the cross-peak is missing from the spectrum for mAb S25-39. Contour lines at a lower level reveal that the cross-peak exists (data not shown here).

the binding pocket of the mAb. The STD TOCSY spectra also exhibited cross-peaks between protons $H8^a$ and $H8'^a$ (Figure 6, a stereospecific assignment of H8*pro*R and H8*pro*S has not been performed yet), showing that these protons were also involved in binding. Protons H8*pro*R^b and H8*pro*S^b were unambiguously identified from the one-dimensional STD NMR spectrum (Figure 5). In summary, the experiments indicate that pyranose unit a of **2** was in immediate contact with the mAbs binding sites and that at least part of the glycosidic linkage was also involved in binding to the proteins.

These results are consistent with our earlier findings for disaccharide **2** bound to mAb S25-2, where intermolecular trNOEs were observed between protons of aromatic amino acids in the binding pocket and protons $H4^a$, $H5^a$, $H5^b$, and $H7^b$ (*12*). At that time, no distinction between protons $H4^a$ and $H5^b$ as well as between protons $H5^a$ and $H7^b$ was possible. From the STD spectra obtained here, it was concluded that protons $H4^a$, $H5^a$, and $H7^b$ were involved in contacts with the protein as explained above. However, the possibility that $H5^b$ may participate in contacts with the protein cannot be ruled out because protons $H4^a$ and $H5^b$ had identical chemical shifts, and $H5^b$ had rather small couplings to both spin−spin coupling partners, $H4^b$ and $H6^b$, making it impossible to observe potential cross-peaks in a STD TOCSY spectrum. Therefore, we cannot decide with certainty whether $H5^b$ is part of the binding epitope of disaccharide **2**.

An interesting observation was made when comparing the region of the protons of the allyl group that blocks the reducing end of disaccharide **2**. Whereas no STD signals were observed for these protons in the complexes of **2** with mAb S25-2 or S25-39, all allylic proton signals were clearly visible in the one-dimensional STD spectrum of **2** in the presence of mAb S23-24. This showed unequivocally that **2** was recognized by mAb S23-24 in a different fashion as compared to those of mAbs S25-2 and S25-39. Nevertheless, the nonreducing pyranose unit a is a common binding epitope, irrespective of the mAb involved.

The results of the STD NMR experiments are visualized in Figure 9, highlighting those protons of **2** that are part of the major binding epitope. To summarize, all mAbs recognized the nonreducing Kdo unit a of **2** as the major portion of the binding epitope.

STD NMR Experiments of α*-Kdo-(2*→*4)-*α*-Kdo-(2*→*O)-allyl **1** Bound to mAbs S25-2, S25-39, and S23-24.* For disaccharide **1**, signal separation is more favorable, and therefore, a more precise epitope mapping with STD NMR was possible. One-dimensional STD NMR spectra and STD TOCSY spectra are shown in Figures 7 and 8. For none of the complexes were STD signals observed originating from protons of the allyl group of **1**. In general, the largest intensities of STD signals were observed for mAb S23-24. Qualitatively, this reflects the results from the ELISA binding assays (Figure 2) that revealed a maximum relative binding affinity for mAb S23-24.

Fortunately, in **1** a distinction between the protons H3 of Kdo units c and b was straightforward. From Figure 7, it is obvious that for all complexes almost exclusively the protons H3 of unit b led to STD signals. Only for the complexes of **1** with mAbs S23-24 and S25-39 were very weak STD signals of protons $H3^c$ identified (Figure 7). This was in accordance with the observation that protons $H3ax^c$ and $H3eq^c$ displayed spin-diffusion-mediated trNOESY cross-peaks to $H6^c$ (cf. discussion above) for mAbs S25-39 and S23-24. For mAb S25-2, these trNOEs were completely absent.

In all cases, the most prominent STD signals were observed for protons $H4^b$, $H5^b$, $H6^b$, $H3ax^b$, and $H3eq^b$. It was concluded that the nonreducing Kdo unit b was in close contact with the antibody binding site. Weak STD signals were observed for protons $H6^c$ and H8*pro*R^b. The most prominent signals in the STD TOCSY spectra were the cross-peaks between $H6^b$ and $H7^b$, independent of the mAb used. This verified that $H6^b$ and $H7^b$ were in contact with protons of the mAb binding pocket. TOCSY cross-peaks between H8*pro*R^b and H8*pro*S^b as well as between H8*pro*R^b and $H7^b$ were weak in all STD TOCSY spectra. This may indicate that the side chain of the nonreducing pyranose ring is not strongly involved in binding. Figure 9 summarizes the results and depicts those protons of **1** that are in contact with the mAb binding sites.

CONCLUSIONS

Our studies furnish a comprehensive representation of the binding modes of two disaccharides, **1** and **2**, that are part of chlamydial LPS to *Chlamydia*-specific mAbs. Utilizing

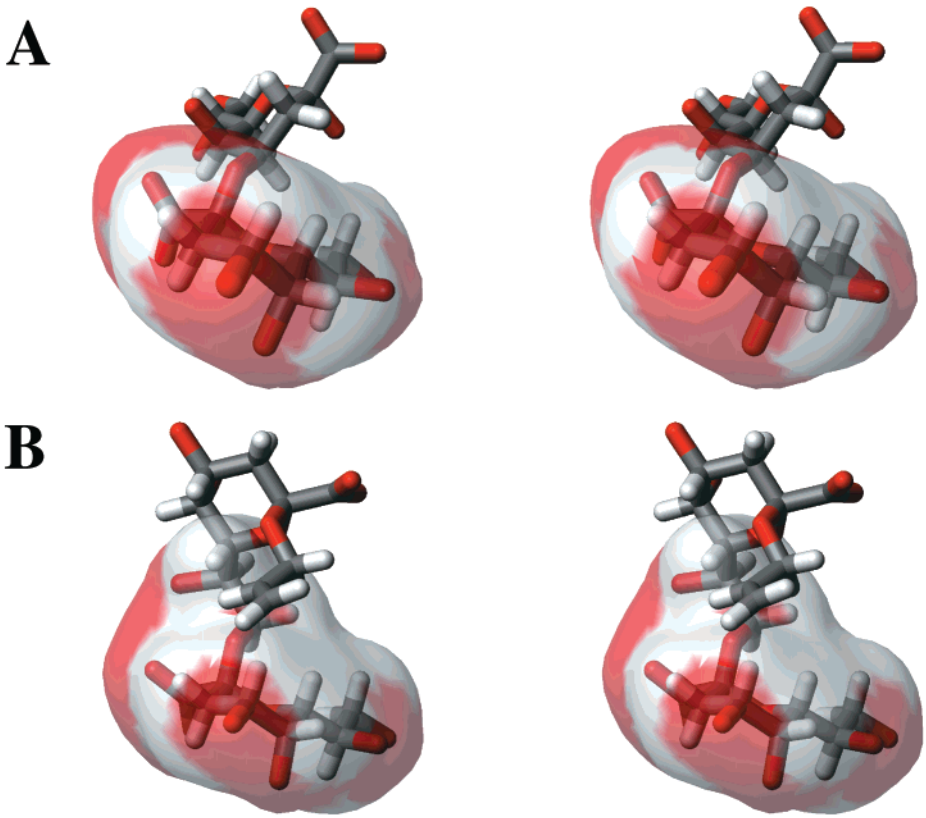

FIGURE 9: Stereopicture of the major binding epitopes of disaccharide **1** (A, conformation A′ is shown) and of disaccharide **2** (B, the conformation found in the crystal sructure is shown) for binding to mAbs S23-24, S25-2, and S25-39. The protons that were found to be in close contact with the protein surface are covered by a soft surface.

QUIET-trNOESY experiments, it was shown that the disaccharides may adopt different bioactive conformations, depending on the mAb. Although it was impossible to perform a quantitative analysis of the bound conformations of the rather flexible disaccharide **2**, our experiments demonstrated that this disaccharide binds to mAbs S25-39, S25-2, and S23-24 in similar bioactive conformations. However, from STD NMR experiments, it became obvious that the binding epitope of **2** when bound to mAb S23-24 was different from the epitope presented to mAb S25-2 or S25-39. The epitope mapping of disaccharide **1** led to less pronounced differences. On the other hand, in this case notably different bioactive conformations were observed upon binding to the mAbs (Table 2). Nevertheless, all six complexes had in common the fact that the most important part for binding to any of the mAbs was the nonreducing Kdo unit (Figure 9). Fine specificity of the molecular recognition was reflected by the amount to which protons from the reducing Kdo unit of **1** or **2** were involved in contacts with protons of the mAb binding pockets.

mAbs S25-2 and S25-39 bound to disaccharide **1** with similar affinities. The bioactive conformation of disaccharide **1** when bound to S25-39 is clearly different from the conformation of **1** bound to S25-2, however. In contrast to the binding to mAb S25-2 (*11*), mAb S25-39 recognized conformation A′ of **1** that was similar to the global minimum energy conformation A (Table 2).

We believe that our results have implications for the classification of mAbs in general, especially if mAbs are to be used for diagnosis or for therapeutic purposes. We propose that NMR experiments lend themselves well to the discrimination of different types of mAbs. In addition to determining the binding affinity of mAbs with classical assays such as ELISA, we suggest obtaining trNOESY and STD NMR spectra to generate "NMR fingerprints" of the corresponding mAb−ligand complexes. Even without a time-consuming analysis of the bioactive conformation of a ligand, such NMR fingerprints will provide valuable information about differences in the individual molecular binding modes. For instance, a simple comparison of one-dimensional STD spectra may already reveal whether two mAbs, or a mAb and a corresponding single-chain F_v fragment, require the same binding epitope of the ligand molecule. One attractive perspective is the extension of this methodology to larger LPS structures from biological sources. Clearly, the technique is not limited to mAb−carbohydrate complexes but is applicable to any type of protein−ligand complex provided that the exchange kinetics allows for the observation of trNOEs and STD effects.

ACKNOWLEDGMENT

The technical assistance of S. Cohrs and M. Willen is gratefully acknowledged. We also acknowledge excellent support from Bruker Analytik GmbH (Rheinstetten, Germany).

SUPPORTING INFORMATION AVAILABLE

trNOESY spectra of disaccharide **2** bound to mAbs S23-24, S25-2, and S25-39, QUIET-trNOE buildup curves for disaccharide **1** bound to mAb S25-39, and pulse programs (Bruker) used for one-dimensional STD NMR experiments

and STD TOCSY NMR experiments. This material is available free of charge via the Internet at http://pubs.acs.org.

REFERENCES

1. Cygler, M., Rose, D. R., and Bundle, D. R. (1991) *Science 253*, 442−445.
2. Bundle, D. R., Baumann, H., Brisson, J.-R., Gagné, S. M., Zdanov, A., and Cygler, M. (1994) *Biochemistry 33*, 5183−5192.
3. Vyas, M. N., Vyas, N. K., Meikle, P. J., Sinnott, B., Pinto, B. M., Bundle, D. R., and Quiocho, F. A. (1993) *J. Mol. Biol. 231*, 133−136.
4. Milton, M. J., and Bundle, D. R. (1998) *J. Am. Chem. Soc. 120*, 10547−10548.
5. Low, D. G., Probert, M. A., Embleton, G., Seshadri, K., Field, R. A., Homans, S. W., Windust, J., and Davis, P. J. (1997) *Glycobiology 7*, 373−381.
6. Moulder, J. W. (1991) *Microbiol. Rev. 55*, 143−190.
7. Caldwell, H. D., and Hitchcock, P. J. (1984) *Infect. Immun. 44*, 306−314.
8. Nurminen, M., Leinonen, M., Saikku, P., and Mäkelä, P. H. (1983) *Science 220*, 1279−1281.
9. Holst, O., Bock, K., Brade, L., and Brade, H. (1995) *Eur. J. Biochem. 229*, 194−200.
10. Brade, H., Brabetz, W., Brade, L., Holst, O., Löbau, S., Lukacova, M., Mamat, U., Rozalski, A., Zych, K., and Kosma, P. (1995) *Pure Appl. Chem. 67*, 1617−1626.
11. Haselhorst, T., Espinosa, J.-F., Jiménez-Barbero, J., Sokolowski, T., Kosma, P., Brade, H., Brade, L., and Peters, T. (1999) *Biochemistry 38*, 6449−6459.
12. Sokolowski, T., Haselhorst, T., Scheffler, K., Weisemann, R., Kosma, P., Brade, H., Brade, L., and Peters, T. (1998) *J. Biomol. NMR 12*, 123−133.
13. Mayer, M., and Meyer, B. (1999) *Angew. Chem. 111*, 1902−1906; *Angew. Chem., Int. Ed. 38*, 1784−1788.
14. Mikol, V., Kosma, P., and Brade, H. (1994) *Carbohydr. Res. 263*, 35−42.
15. Fu, Y., Baumann, M., Kosma, P., Brade, L., and Brade, H. (1992) *Infect. Immun. 60*, 1314−1321.
16. Holst, O., Broer, W., Thomas-Oates, J. E., Mamat, U., and Brade, H. (1993) *Eur. J. Biochem. 214*, 703−710.
17. Brade, L., Zych, K., Rozalski, A., Kosma, P., Bock, K., and Brade, H. (1997) *Glycobiology 7*, 819−827.
18. Kosma, P., Gass, J., Schulz, G., Christian, R., and Unger, F. M. (1987) *Carbohydr. Res. 167*, 39−54.
19. Bradford, M. M. (1976) *Anal. Biochem. 72*, 248−254.
20. Scherf, T., and Anglister, J. (1993) *Biophys. J. 64*, 754−761.
21. Vincent, S. J. F., Zwahlen, C., Post, C. B., Burgner, J. W., and Bodenhausen, G. (1997) *Proc. Natl. Acad. Sci. U.S.A. 94*, 4383−4388.
22. Neidig, K.-P., Geyer, M., Görler, A., Antz, C., Saffrich, R., Beneicke, W., and Kalbitzer, R. (1995) *J. Biomol. NMR 6*, 255−270.
23. Klein, J., Meinecke, R., Mayer, M., and Meyer, B. (1999) *J. Am. Chem. Soc. 121*, 5336−5337.
24. Vogtherr, M., and Peters, T. (2000) *J. Am. Chem. Soc. 122*, 6093−6099.
25. Herfurth, L., Weimar, T., and Peters, T. (2000) *Angew. Chem. 112*, 2192−2194; *Angew. Chem., Int. Ed. 39*, 2097−2099.
26. Stuike-Prill, R., and Meyer, B. (1990) *Eur. J. Biochem. 194*, 903−919.
27. Peters, T., Meyer, B., Stuike-Prill, R., Somorjai, R., and Brisson, J.-R. (1993) *Carbohydr. Res. 238*, 49−73.
28. Arepalli, S. R., Glaudemans, C. P., Daves, G. D., Kovac, P., and Bax, A. (1995) *J. Magn. Reson., Ser. B 106*, 195−198.
29. Moseley, H. N. B., Curto, E. V., and Krishna, N. R. (1995) *J. Magn. Reson., Ser. B 108*, 243−261.
30. Ni, F., and Zhu, Y. (1994) *J. Magn. Reson., Ser. B 102*, 180−184.

BI000780O